Chronic administration of saturated fats and fructose differently affect SREBP activity resulting in different modulation of Nrf2 and Nlrp3 inflammasome pathways in mice liver

(Article begins on next page)

13 July 2024

Chronic administration of saturated fats and fructose differently affect SREBP activity resulting in different modulation of Nrf2 and Nlrp3 inflammasome pathways in mice liver

Nigro D[1], Menotti F[1], Cento A[1], Serpe L[2], Chiazza F[2], Dal Bello F[3], Romaniello F[3], Medana C[3], Collino M[2], Aragno M[1], Mastrocola R[1*].

[1]Department of Clinical and Biological Sciences, University of Turin, Italy; [2]Department of Drug Science and Technology, University of Turin, Italy; [3]Department of Molecular Biotechnology and Health Sciences, University of Turin, Italy.

Running title: SREBP affects Nrf2and Nlrp3

*Corresponding author:

Raffaella Mastrocola
Department of Clinical and Biological Sciences,
University of Turin
Corso Raffaello 30
10125 Turin, Italy.
Tel. +39 011 6707758
Fax +39 011 6707753
e-mail address: raffaella.mastrocola@unito.it

Abbreviations: ACC, acetyl CoA carboxylase; ApoB, apolipoprotein B; COX-1, cytochrome c oxidase subunit 1; CPT1-l, carnitine palmitoyltrasnferase; FAS, fatty acid synthase; GAPDH, glyceraldehyde-3-phosphate dehydrogenase; GCLC, glutamate-cysteine ligase catalytic; GCLM, glutamate-cysteine ligase catalytic modifier; Gsta, glutathione S-transferase class Alpha; HMG-CoA-R, hydroxy-3-methylglutaryl coenzyme A reductase; ICAM-1, intercellular adhesion molecule 1; IL-1β, interleukin-1 beta; Keap1, kelch-like ECH-associated protein 1; MnSOD, manganese-dependent superoxide dismutase; MPO, myeloperoxidase; NFkB, nuclear factor-kappa B; Nlrp3, Nod-like receptor protein 3; Nrf2, nuclear factor (erythroid-derived 2)-like 2; Nqo1, NAD(P)H:quinone oxidoreductase-1; PGC1-α, peroxisome proliferator-activated receptor gamma coactivator 1-alpha; SCAP, SREBP cleavage-activating protein; SDH-A, succinate dehydrogenase subunit A; SREBP1, sterol regulatory element-binding protein 1; SREBP2, sterol regulatory element-binding protein 2.

Abstract

The overconsumption of both saturated fats and fructose in the modern society has been related to the development of non-alcoholic fatty liver disease (NAFLD). However, the specific contribution of individual dietary components on the progression of NAFLD to non-alcoholic steatoepatitis (NASH) has been poorly investigated.

Therefore, the aim of our study was to investigate the dissimilar effects of these two dietary components on selected proinflammatory and antioxidant pathways in the liver of C57BL/6 mice fed a standard (SD), a 45% saturated fat (HFAT), or a 60% fructose (HFRT) diet for 12 weeks. HFAT diet evoked systemic metabolic alterations and overweight, not observed in HFRT mice. However, HFRT mice had a greater hepatic triglyceride deposition with increased ratio of triacylglycerols containing the palmitic acid compared to HFAT, as assessed by LC-MS analysis. This effect is due to the higher activation of the SCAP/SREBP1c lipogenic pathway by HFRT feeding. In addition, we found inhibition of Keap1/Nrf2 antioxidant signaling and more robust stimulation of the Nlrp3 inflammasome pathway in the livers of HFRT-fed mice when compared with HFAT-fed mice, which is consistent with the recent finding that palmitate and SREBP1c are implicated in hepatic oxidative stress and inflammation. These effects were associated with increased hepatic inflammation, as confirmed by high expression of markers of leukocyte infiltration in the HFRT group. Thus, we hypothesize an amplifying loop among lipogenesis, palmitate, Nrf2 and Nlrp3 that leads to a higher risk of NAFLD progression to NASH in a high-fructose diet compared to a high-saturated fat intake.

Keywords: fructose; saturated fat; NAFLD; SREBP1c; Nlrp3 inflammasome; Nrf2.

1. Introduction

Non-alcoholic fatty liver disease (NAFLD) is the most frequent chronic liver disease, affecting about 25% of the western world population [1], and represents the hepatic manifestation of the metabolic syndrome, also characterized by insulin resistance, dyslipidemia, hypertension, type 2 diabetes and overweight [2,3] . The prevalence of both metabolic syndrome and NAFLD is rapidly increasing in western countries due to changes in dietary habits, that comprise the rising consumption of saturated fats and fructose [4,5]. Consistently, general over-nutrition, particularly when rich in fats and/or sugars, is being discussed to be a key factor in the development of NAFLD [6]. Although it is reasonable to propose that over-consumption of either fats or carbohydrates is an important threat that may promote the development of NAFLD [7], a lot of studies reported that dietary composition may be critical in hepatic fat deposition [8-10]. In NAFLD the characteristic hepatic accumulation of lipids is mainly due to (i) excessive influx of fatty acids in the liver from endogenous fat depots, (ii) excess dietary fat intake and (iii) *de novo* lipogenesis [7]. In this regard, dietary fats and carbohydrate contribute to lipid deposition in the liver through direct lipid influx and *de novo* lipid synthesis from sugar, respectively. These different mechanisms for lipids accumulation induced by fats or sugars may in turn differently affect other events which have been recently involved in insulin resistance and NAFLD onset, such as mitochondrial dysfunction and endoplasmic reticulum stress [11].

A relevant aspect to be taken into consideration is that 5-10% of NAFLD evolve in non-alcoholic steatohepatitis (NASH). To date, the molecular mechanisms and pathological events underlying the progression of NAFLD to NASH are still not completely cleared. However, most recently evidence suggests a key role for the activation of selective molecular pathways leading to development of an excessive inflammatory response [12]. One of the molecular factors recently demonstrated to be involved by both *in vitro* and *in vivo* models is the nuclear factor E2-related factor 2 (Nrf2) [13,14].

It is known that Nrf2 regulates antioxidant genes, as well as those for detoxifying enzymes. In addition, Nrf2 has been recently suggested to have a role in the prevention of NASH by both repressing the expression of genes involved in lipid synthesis and enhancing β-oxidation [15-17]. The activity of Nrf2 has been in turn linked to that of the NOD-like receptor family pyrin domain-containing protein inflammasome (Nlrp3), a multi-protein platform responsible for the activation of early innate inflammatory processes. Indeed, very recent studies have reported a tight correlation between enhanced activity of Nrf2 and inhibition of Nlrp3 signaling in the liver, and this Nrf2-mediated inflammasome modulation has been proved to reduce both acute toxic liver injury and fibrosis [18-20].

However, the specific contribution of individual dietary components on the modulation of these selected molecular pathways and, thus, the progression of NAFLD to NASH have been poorly investigated, so far. In this perspective, the present study aims to highlight the different impact of two relevant components of the western diet, saturated fats and fructose, on hepatic lipid metabolism and fatty acids deposition, focusing on the Nrf2 and Nlrp3 molecular pathways activation.

2. Materials and Methods

2.1 Animals and treatments

Male C57Bl/6j mice (Charles River Laboratories, Calco, Italy) of 4 weeks of age were cared for in compliance with the European Council directives (No. 86/609/EEC) and with the Principles of Laboratory Animal Care (NIH No. 85–23, revised 1985). The scientific project was approved by the Ethical Committee of the Turin University (permit number: D.M. 94/2012-B). Mice were fed a standard diet (SD group, $n = 8$), a 45% fat diet (HFAT group, $n = 10$) or a 60% fructose diet (HFRT group, $n = 10$) for twelve weeks. Standard diet (Research Diets, New Brunswick, NJ, USA, D12450K) composition was: 70% of calories in carbohydrates (55% from corn starch and 15% from maltodextrin), 10% of calories in fat (5% from soybean, 5% from lard), and 20% of calories

from proteins. High-fat pelleted chow (Research Diets, D12451) composition was: 35% of calories in carbohydrates (7% from corn starch, 10% from maltodextrin, and 17% from fructose), 45% of calories in fat (5% from soybean, 40% from lard), and 20% of calories from proteins. High-fructose pelleted chow (Research Diets, D02022704) composition was: 70% of calories in carbohydrates (10% from corn starch and 60% from fructose), 10% of calories in fat (5% from soybean, 5% from lard), and 20% of calories from proteins. All groups received drink and food *ad libitum*.

2.2 Oral Glucose Tolerance Test

One day before the mice were due to be killed, the oral glucose tolerance test (OGTT) was performed after a fasting period of 6 h by administering glucose (2 g/kg) by oral gavage. Once before administration and 15, 30, 60, and 120 min afterward, blood was obtained from the saphenous vein, and glucose concentration was measured with a conventional Glucometer (GlucoGmeter, Menarini Diagnostics, Florence, Italy).

2.3 Procedures and plasma analyses

Body weight and food intake were recorded weekly. Fasting glycemia was measured at the start of the protocol and every 4 weeks by saphenous vein puncture using a glucometer (GlucoGmeter, Menarini Diagnostics). After 12 weeks, mice were anesthetized and killed by cardiac exsanguination. Blood was collected and the liver was rapidly removed. Plasma and tissue lipid profile was determined by standard enzymatic procedures using reagent kits (Hospitex Diagnostics, Florence, Italy). Plasma insulin level was measured using an enzyme-linked immunosorbent assay (ELISA) kit (Mercodia AB, Uppsala, Sweden).

A portion was cryoprotected in OCT (Optimal Cutting Temperature) compound (VWR, Milan, Italy) and frozen in N2 for cryostatic preparations. Other portions were frozen in N2 and stored at -80°C for protein analysis.

2.4 Oil Red O staining

Liver lipid accumulation was evaluated by Oil Red O staining on 7μm cryostatic sections. Stained tissues were viewed under an Olympus Bx4I microscope (20x magnification) with an

AxioCamMR5 photographic attachment (Zeiss, Gottingen, Germany).

2.5 HPLC-HRMS settings for TAGs analysis

An Ultimate 3000 Dionex, Thermo Scientific (Milan, Italy) HPLC instrument coupled through an APCI source to an LTQ Orbitrap Thermo Scientific mass analyzer were used.

TAGs analysis were performed as previously described [20].

Briefly a first method involves the use of two Luna C18(2) (Phenomenex) columns (150 × 2.1 mm,3 μm particle size) in series and a gradient of acetonitrile (solvent A) and dichloromethane (solvent B).

The second separation method make use of a Develosil C30 column (150 × 2.0 mm, 5 μm particle size, Phenomenex) with acetonitrile and dichloromethane as eluents. The LC column effluent entered the APCI source with nitrogen as the sheath and auxiliary gas. The source voltage was set to 4.1 kV. The heated capillary temperature was maintained at 250 °C. The main parameters adopted were: vaporizer temperature 450 °C, discharge current 5.00 μA, capillary voltage 10.00 V, tube lens 40 V. High resolution accurate mass analysis (HRAM) was used to reliably identify precursor ions of different TAGs and to characterize their neutral losses. High resolution spectra were acquired with a resolution of 60000 (FWHM) and the mass accuracy of recorded ions (vs. calculated) was ± 2 millimass units (without internal calibration). MS^n spectra were acquired in the range between the ion trap cut-off and precursor ion *m/z* values. Triacylglycerols (TAGs) were identified as reported [21] and quantified using a triacylglycerol standard curve .

2.6 Preparation of tissue extracts

Cytosolic and nuclear extracts were prepared as previously described [22]. Briefly, livers were homogenized at 10% (wt/vol) in a Potter Elvehjem homogenizer (Wheaton, Millville, NJ) using a homogenization buffer containing 20 mM HEPES (pH 7.9), 1 mM MgCl2, 0.5 mM EDTA, 1% Nonidet P-40, 1 mM EGTA, 1 mM DTT, 0.5 mM PMSF, 5 μg/ml aprotinin, 2.5 μg/ml leupeptin and 2 mM NaVO3. Homogenates were centrifuged at 1000g for 5 min at 4°C. Supernatants were removed and centrifuged at 105,000g at 4 °C for 40 min to obtain the cytosolic fraction. The

pelleted nuclei were resuspended in extraction buffer containing 20 mM HEPES (pH 7.9), 1.5 mM MgCl2, 300 mM NaCl, 0.2 mM EDTA, 20% glycerol, 1 mM EGTA, 1 mM DTT, 0.5 mM PMSF, 5 µg/ml aprotinin, 2.5 µg/ml leupeptin and 2 mM NaVO3 and incubated on ice for 30 min for high-salt extraction, followed by centrifugation at 15,000g for 20 min at 4 °C. The resulting supernatants containing nuclear proteins were carefully removed. Protein content was determined using the Bradford assay (BioRad, Hercules, CA, USA). Protein extracts were stored at −80°C until use.

2.7 Western blotting

Equal amounts of proteins were separated by SDS-PAGE and electrotransferred to nitrocellulose membrane (GE-Healthcare Europe, Milano, Italy). Membranes were probed with primary antibodies, listed in Supplemental material, followed by incubation with appropriated HRP-conjugated secondary antibodies (BioRad).

Proteins were detected with Clarity Western ECL substrate (BioRad) and quantified by densitometry using analytic software (Quantity-One, Bio-Rad). For each analyzed protein western blotting was peformed in duplicate for all the available samples (SD = 8; HFAT = 10; HFRT = 10). Results were normalized with respect to densitometric value of mouse anti-GAPDH (Santa Cruz Biotechnology) for cytosolic and mouse anti-histone H3 (Abcam) for nuclear proteins and then expressed as fold of SD value.

2.8 Respiratory complex activities

The mitochondrial respiratory chain complexes enzymatic activities were checked on liver homogenates by spectrophotometric assays as described by Spinazzi et al. [23] and the results were normalized to the protein content. Briefly, the activity of complex I (NADH:ubiquinone oxidoreductase) was evaluated by using ubiquinone as the electrons acceptor and NADH as donor and following the decrease of absorbance at 340 nm for 5 min resulting from the oxidation of the ubiquinone. The assay for activity of complex II (succinate dehydrogenase) involves dichlorophenolindophenol (DCPIP) as the electrons acceptor and succinate as donor. The activity is then evaluated by the decrease of absorbance at 590 nm for 20 minutes. For complex III

(decylubiquinol cytochrome c oxidoreductase) the oxidized cytochrome c was used as the electrons acceptor and decylubiquinol as donor and the assay was performed following the increase in absorbance at 550 nm resulting from the reduction of cytochrome c. Finally, the activity of complex IV (cytochrome c oxidase) was checked following the decrease in absorbance at 550 nm resulting from the oxidation of reduced cytochrome c, which is the electrons donor, and was expressed as nmol min−1 mg−1 of total proteins (extinction coefficient for reduced cytochrome c 18.5 mM−1 cm−1). The specificity of complex IV activity was confirmed by the inhibition with potassium.

2.9 RT-PCR analysis

Total RNA was extracted from liver samples using the AllPrep® DNA/RNA/protein Kit (Quiagen, Hilden, Germany), according to the manufacturer's instructions. The total RNA concentration (μg/mL) was determined by the fluorometer Qubit and the Quant-iT™ RNA Assay Kit (Invitrogen, Milano, Italy). A total of 500 ng of RNA was reverse-transcribed using QuantiTect Reverse Transcription Kit (Qiagen), The synthesized cDNA was used for real-time polymerase chain reaction (PCR). The cDNA was amplified by real-time PCR using SsoFast™ EvaGreen (Bio-Rad,) and primers (Sigma) specific for glutathione S-transferase class Alpha (Gsta1 and Gsta2), glutamate-cysteine ligase catalytic (GCLC) and modifier (GCLM) subunits, NAD(P)H:quinone oxidoreductase-1 (Nqo1), acetyl coenzyme A carboxylase (ACC), fatty acid synthase (FAS), and hydroxyl methyl glutaryl coenzyme A reductase (HMG-CoA-R). Primers sequences are listed in Supplemental material. The PCR reaction was performed at 95°C for 30s followed by 40 cycles of 95°C for 5s, 55°C for 10s. All samples were run in duplicate. At least two nontemplate controls were included in all PCR. The transcript of the reference gene ribosomal RNA 18S (Mm_Rn18s_3_SG, cat. no. QT02448075) was used to normalize mRNA data, and the quantification data analyses were performed by using the Bio-Rad CFX Manager Software, version 1.6 (Bio-Rad) according to the manufacturer's instructions.

2.10 Glutathione assay

Oxidized-to-reduced glutathione ratio (GSSG/GSH) was assessed by the method of Owens and Belcher [24]. A mixture was directly prepared in a 96-wells microplate: 0.05 M Na-phosphate buffer (pH 7.0), 1 mM EDTA (pH 7.0), and 10 mM dithionitrobenzoic acid plus an aliquot of the sample. GSH content was evaluated after 2 min at 412 nm and expressed as μg/mg protein. Suitable volumes of diluted glutathione reductase and of reduced nicotinamide adenine dinucleotide phosphate were then added to evaluate the total glutathione level. The difference between total glutathione and GSH content represents the GSSG content (expressed as μg/mg protein).

2.11 Immunofluorescence

Nrf2 subcellular localization was analyzed by immunofluorescence on 7 μm liver cryostatic sections. After blocking, sections were incubated overnight with a rabbit anti-Nrf2 (Thermo Scientific, Code# PA5-27889) and subsequently for 1h with TRITC-conjugated secondary antibody. Nuclei were counterstained with Hoechst dye. Sections were visualized using an Olympus epifluorescence microscope (Olympus Bx4I) at 40x magnification, digitised with a high resolution camera (Zeiss), and colour-combined with Adobe Photoshop (Adobe System, San José, CA, USA).

2.12 Immunohistochemistry

Neutrophils infiltration was analyzed by immunohistochemistry on 7 μm liver cryostatic sections. After blocking, sections were incubated overnight with a rabbit anti-MPO antibody (Abcam, Code# 9535) and subsequently for 1h with HRP-conjugated secondary antibody. Immunoreactivity was evidenced by reaction with 3,3'-diaminobenzidine substrate and nuclei were counterstained with hematoxylin. Micrographs were acquired using an Olympus microscope at 10x/20x magnification.

2.13 Statistical analysis

The Shapiro-Wilk test was used to assess the normality of the variable distributions. One-way ANOVA followed by Bonferroni's post-hoc test were adopted for comparison among the four groups of animals. Data were expressed as mean ± standard deviation. Threshold for statistical

significance was set to $P<0.05$. Statistical tests were performed with GraphPad Prism 6.0 software package (GraphPad Software, San Diego, CA, USA).

2.11 Materials

All compounds were purchased from Sigma Chemical Co. (St. Louis, MO, USA), unless otherwise stated.

3. Results

3.1 General parameters

Although in the three groups of animals no difference in food intake was detected (Table 1), the HFAT diet supplied a significantly higher daily calories intake, which was in great part due to the contribution of saturated fats (lard), even if a little percentage of calories was derived from sugars (sucrose). Instead, in the HFRT diet the daily calories intake was almost exclusively derived from fructose (Table 1).

At the end of the experimental protocol, only HFAT mice showed a marked increase in body weight, epididymal adipose tissue weight, and insulinemia in association with a significant reduction in liver weight, in comparison to SD and HFRT mice (Table 2). While, both the HFAT and the HFRT diets induced significant increases in plasma fasting glucose, triglyceride and cholesterol levels (Table 2) and altered OGTT curve (Fig. 1), in comparison to SD. Nevertheless, all these parameters were altered to a larger extent by the HFAT diet.

3.2 HFAT and HFRT diets altered hepatic lipid content.

In liver slices from HFAT and HFRT mice we detected a relevant lipid deposition compared to SD (Fig. 2a), with a diffuse microvescicular distribution in the HFAT group and a macrovescicular periportal distribution in HFRT group. Consistently, although both diets significantly increased TG liver content with respect to SD, HFRT mice liver accumulated more TG compared to HFAT mice (+25%), whereas hepatic cholesterol levels slightly increased in both diets, without reaching statistical significance (Fig. 2b).

10

3.3 HFAT and HFRT diets differently affected liver fatty acids export and oxidation

ApoB100 protein level was measured in liver as a marker of VLDL assembly (Fig. 3a). No significant difference was seen in HFAT diet, while a significant increase in HFRT livers (+60% vs SD; +45% vs HFAT) indicated enhanced VLDL production, resulting in increased TAGs export. In contrast, HFAT mice showed decreased intensity in the expression of CPT1-L (-20% vs SD) indicating reduced rate of β-oxidation (Fig. 3b), of PGC-1α (-40% vs SD), the major regulator of mitochondrial biogenesis (Fig. 3c), and of the enzyme SDH-A (-20% vs SD), part of complex II in the mitochondrial respiration (Fig. 3d), while the enzyme COX-1 (Fig. 3d), a component of complex IV, was upregulated (+120% vs SD). HFRT diet induced in liver a significant increase in mitochondrial β-oxidation (Fig. 3b), and SDH-A and COX-1 expression (+20% and +160%, respectively, vs SD) (Fig. 3d), without affecting mitochondrial biogenesis (Fig. 3c).

3.4 HFAT and HFRT diets differently impaired mitochondrial respiratory complex activity

To thoroughly investigate the different impact of the HFAT and HFRT diets on mitochondrial efficiency, we analyzed the enzymatic activities of the four complexes of the mitochondrial respiration. The HFAT diet downregulated only complex I when compared to SD (-22%) (Fig. 4a), whereas HFRT diet significantly upregulated all the examined complexes (Fig. 4a-d), indicating an enhancement of mitochondrial respiration.

3.5 HFAT and HFRT diets altered triacylglycerols (TAGs) composition

LC-MS analysis on liver homogenates did not detect significant alterations in the relative proportion of different TAGs in the HFAT group, whereas an altered ratio between TAGs containing saturated (palmitic and stearic) or unsaturated (oleic, linoleic, linolenic) fatty acids was found in HFRT mice (Table 3). Most notably, in HFRT mice the TAGs containing the unsaturated oleic acid were decreased (L-Ln-O: -30% vs SD, -40% vs HFAT; O-O-S: -21% vs SD, -36% vs HFAT), while many of those containing the saturated palmitic acid were significantly increased (P-

11

L-O: +180% vs SD and HFAT; O-O-P: +50% vs SD and HFAT; P-O-S: +20% vs SD; +10% vs HFAT).

3.6 HFAT and HFRT diets differently impact on lipogenesis

Since in HFRT mice we observed an increase in TAGs containing the palmitic acid, which is the primary fatty acid produced during *de novo* lipogenesis, we assessed the expression and the activation of the transcription factors SREBP1, that regulates fatty acids synthesis, and SREBP2, that regulates cholesterol synthesis, and the expression of their main target genes. In HFRT mice the SREBPs activating protein SCAP was markedly upregulated (+90% vs SD; +80% vs HFAT) (Fig. 5a). Moreover, the HFRT diet induced the 125-kDa precursor of SREBP1c upregulation (+65% vs SD) and the cytosolic 68-kDa active form was decreased in intensity (-53% vs SD) paralleled by the increase in the nuclear active form (+52% vs SD), indicating a marked activation of SREBP1 signaling (Fig. 5b). We then analyzed two of the main SREBP1c target genes. As a consequence of SREBP1c activation, we observed in HFRT mice a significant hyperexpression and activation of ACC, as revealed by mRNA and protein levels, and by the ratio ACC/pACC (with pACC representing an inactive post-translationally modified form), and increased mRNA and protein expression of FAS (Fig. 5c). Conversely, HFAT mice showed a slight, but not significant, increase in SREBP1 expression (+33% vs SD) and translocation from cytosol to nucleus (nuclear active form +15% vs SD) (Fig. 5b), that barely affected FAS expression (Fig. 5c).

The HFAT diet was able to induce cholesterologenesis through the activation of SREBP2 (nuclear active form +20% vs SD) and the hyperexpression of the rate-limiting enzyme of cholesterologenesis HMG-CoA-R. However, activation of SREBP2 was markedly higher in the HFRT diet (nuclear active form +60% vs SD; +33% vs HFAT), as well as the mRNA and protein expression of HMG-CoA-R (Fig. 5e).

3.7 HFAT and HFRT diets differently affect antioxidant response

The upregulation of mitochondrial oxidative metabolism observed in HFRT mice could suggest alterations in oxidative markers and mitochondrial antioxidant defenses.

We thus evaluated the hepatic activation level of the antioxidant transcription factor Nrf2 and the expression of its inhibitor Keap1. Since Nrf2 is reported to migrate with an apparent molecular weight of 110 kDa, even though it has a calculated molecular mass of about 68 kDa [25], we reported a representative blot that encompasses the 50-kDa through to 150-kDa range to allow all possible candidate bands to be viewed (Fig. 6a). The robust hyperexpression of Keap1 in the HFRT mice (+55% vs SD and HFAT) is likely to retain Nrf2 in the cytosol, as shown by the band at 110 kDa. Accordingly, in the nuclear extracts we detected a reduced intensity of both the bands at 110 and 68 kDa in the HFRT group. The reduced nuclear translocation of Nrf2 evoked by the diets, especially by the HFRT diet, was confirmed by immunofluorescence analysis (Fig. 6b). In the liver sections from SD mice Nrf2 was mainly localized in the nuclei, with a partial diffused distribution in the cytosol. In contrast, the Nrf2 nuclear localization was reduced in the HFAT, and almost completely disappeared in the HFRT mice liver. Interestingly, in both HFAT and HFRT mice livers Nrf2 was accumulated along the plasmamembranes. As consequence of inhibited Nrf2 nuclear translocation, the gene expression of the main targets of Nrf2 (Gsta1, Gsta2, GCLC, GCLM, and Nqo1) was downregulated, achieving statistical significance only in the HFRT mice (Fig. 6c). Moreover, since Nrf2 target genes are involved in GSH-recycling, we observed an increased ratio of GSSG/GSH, index of oxidative imbalance, that was significant only in HFRT mice (+43% vs SD; +12% vs HFAT) (Fig. 6d).

3.8 HFAT and HFRT diets differently induced inflammatory response

We finally investigated Nlrp3 expression and its downstream signaling, shown by pro-caspase-1 cleavage and IL-1β production, that were upregulated in both diets (Fig. 7a-c). However, Nlrp3 was markedly hyperexpressed in HFRT liver compared to both SD and HFAT (+100% vs SD; +54% vs HFAT) (Fig. 7a), as well as the downstream signaling (active caspase-1: +50% vs SD; +25% vs HFAT; IL-1 β: +90% vs SD; +46% vs HFAT) (Fig. 7b-c). Conversely, NFkB p65 was largely translocated from cytosol to nucleus in the liver of both HFAT and HFRT group (Fig. 7d). As consequence of proinflammatory signaling, the hepatic level of ICAM-1 was significantly increased

13

only in the HFRT mice (+40% vs SD; +27% vs HFAT) (Fig. 8a), and the neutrophils infiltration evaluated by immunohistochemistry for MPO on liver sections was evidenced in both diets, but to a larger extent in the HFRT group (Fig. 8b).

4. Discussion

Several epidemiological studies have revealed that a diet rich in fat and cholesterol may increase the odds to develop NAFLD [26]. Most recently, similar data have also been reported for a high dietary intake of sugar and in particular of fructose [27]. For this reason, the role of the rising consumption of fats and fructose in human diet in the development of NAFLD and insulin resistance has recently attracted much interest [28-30]. A recent work showed that both diets rich in fat and fructose lead to liver steatosis over time [10] and a combined feeding of these two macronutrients was found to exacerbate the damaging effect of the single components [7].

We must underlie that in the present study the higher caloric contribution of the HFAT diet compared to the HFRT diet may account for the greater weight gain and adipose tissue expansion. The different caloric intake of the two diets may thus affect some of the systemic parameters here analyzed. However, when considering the hepatic outcomes of dietary manipulation, despite lower caloric intake, the HFRT diet led to a more severe steatosis and more pronounced pro-oxidant and pro-inflammatory signaling activation with respect to the HFAT diet. Indeed, we here demonstrate that the HFAT diet alters the systemic glucose and lipid metabolism to a greater extent than the HFRT diet, whereas a greater hepatic TG deposition is detected in HFRT mice when compared to HFAT mice. This is in agreement with ours and other authors studies showing the induction of ectopic tissues lipid deposition by fructose, both in human and in rodent, without affecting body weight and adiposity [22,31-34].

Our results indicate that saturated fats and fructose in the diet exert dissimilar effects on liver lipid metabolism. We show that hepatic lipid accumulation in HFAT mice is due to the lack of induction of both mitochondrial oxidation and lipid export in response to increased dietary lipids supply that

mainly accumulate in adipose depots and increase plasma TG and cholesterol levels, and finally reach the liver in a moderate amount. In contrast, the increased mitochondrial metabolism and ApoB100 hyperexpression induced by HFRT diet do not explain the relevant liver lipid deposition detected, which is consequence of a local alteration in hepatic lipid metabolism only partially affecting systemic parameters. In animal models of obesity a reduced rate of fatty acid oxidation is frequently reported [35,36] and it is largely demonstrated that activating β-oxidation decreases hepatic lipid accumulation and improves insulin sensitivity [37]. Conversely, mice subjected to a long-term high-fructose feeding showed an increase in skeletal muscle mitochondrial efficiency, with our results in agreement with previous studies [38]. Additionally, in a human study that enrolled ninety-seven subjects to consume beverages sweetened with increasing concentrations of high-fructose corn syrup, an increased fasting and/or postprandial plasma concentration of ApoB was observed [39], indicating enhanced export of triglycerides from liver to plasma.

Furthermore, it has been demonstrated that if a high-fat feeding induces a direct extrahepatic lipid supply, paralleled by reduced fatty acids export and metabolism, high-fructose intake strongly increases hepatic lipogenesis [11]. We have previously documented this paradoxical stimulation of lipogenesis by fructose, showing that the dysregulation of the SREBP signaling was related to the glycation of SCAP induced by fructose-derived advanced glycation end-products [22,31]. Here we evaluated the contribution of the *de novo* lipogenesis to the liver fatty acids deposition through the analysis of the SCAP/SREBP lipogenic pathway in the two diets and the results confirmed that fructose has a higher lipogenic power than fats, being both SREBP1c and SREBP2 pathways activated to a greater extent in the liver of fructose-fed mice compared to fat-fed mice.

An original contribution of the present study is the LC-MS analysis of TAGs in liver homogenates showing that the levels of many TAGs containing the palmitic acid were drastically higher in liver of HFRT mice when compared to liver of both SD and HFAT littermates. This observation strengthens the differences we recorded in terms of lipogenesis as palmitate (C16:0) is the primary fatty acid endogenously synthesized through the *de novo* lipid synthesis regulated by SREBP1c

15

activation [40], and it can activate in turn cholesterol synthesis via SREBP2 stimulation in HepG2 cells [41]. High levels of palmitic acid have been also reported to induce inflammation, ER stress and insulin-resistance [42,43]. For instance, a human research on 3004 randomly sampled healthy people positively linked circulating palmitic acid to adiposity, triglycerides, inflammation biomarkers, and insulin resistance [44]. Palmitic acid is one of the most well characterized DAMPs leading to Nlrp3 inflammasome activation in the liver, which significantly contributes to the progression of the diet-induced steatohepatitis [45,46]. One of the major pathways so far implicated in hepatic Nlrp3 inflammasome activation involves the recruitment of different types of TLRs and MyD88, the common TLR adaptor. Besides, the TLR4/MyD88-mediated activation of Nlrp3 inflammasome has been recently demonstrated to be critical for the development of dietary steatohepatitis [47]. We previously documented that the pharmacological inhibition or the genetic ablation of Nlrp3 reduces liver and kidney dysfunctions and fibrosis markers in mice fed fructose-containing diets [48,49]. Here we demonstrated, for the first time, that HFRT diet induced markedly increased hepatic levels of Nlrp3, caspase-1 and IL-1β, ICAM-1 and neutrophils infiltration, while in HFAT diet inflammasome signaling was activated to a significantly lesser extent accompanied by less intense inflammatory response. Intriguingly, recent studies have suggested a new role for SREBPs in the induction of inflammasome, but the molecular mechanisms by which SREBPs regulate the inflammasome and innate immunity remain to be elucidated [50,51]. In particular macrophages from SREBP-1a deficient mice failed to activate lipogenesis as well as inflammasome hallmarks, caspase-1 activation and IL-1β secretion [50]. Moreover, in human umbilical vein endothelial cells the SREBP2-activated Nlrp3 inflammasome causes functionally disturbed endothelium with increased inflammation [51].

SREBP1 was also associated to the Nrf2-regulated antioxidant response. Nrf2 seems to protect the liver against steatosis by inhibiting lipogenesis and promoting fatty acid oxidation [52]. In fact, Nrf2-KO mice have increased mRNA expression levels of cholesterologenic transcriptional factors and lipogenesis related genes, including SREBP1, FAS, and ACC in the liver, compared to wild

type mice fed a high-fat diet for 16-20 weeks, and are thus prone to develop diet-induced hepatosteatosis and progress to a more severe NASH [13]. On the other hand, saturated fatty acids, in particular palmitate, modulate Nrf2 expression and activation. A dose- and time-dependent increase in Nrf2 protein level has been observed in two different studies on cultured hepatocytes exposed to palmitate, correlated with proliferation and abnormal hepatic metabolizing enzymes [53,54], although no information on nuclear activation was reported. However, in human umbilical vein endothelial cells, as well as in primary human hepatocytes, palmitate treatment markedly inhibited Nrf2 nuclear translocation and transcriptional activity [14,55]. Consistently, in our model of diet-induced NAFLD, we observed increased levels of cytosolic Nrf2 and of its inhibitor Keap1, paralleled by impaired Nrf2 nuclear translocation in the HFRT group, where a greater activation of the SCAP-SREBP lipogenic pathway was also detected. As previously demonstrated in the liver of Nrf2^{-/-} mice, the loss of Nrf2 transcriptional activity leads to the downregulation of genes specifically involved in GSH-mediated detoxification processes and GSH recycling, exposing mice to increased oxidative stress damage [56]. Accordingly, the lower Nrf2 nuclear translocation observed in the liver of HFRT mice was paralleled by reduced expression of its target genes Gsta1, Gsta2, GCLC, GCLM, and Nqo1, and increased GSSG/GSH ratio, and was related to the higher SREBP1c activation and palmitate-containing TAGs accumulation, in comparison to HFAT mice.

In addition, Nrf2 may play a pivotal role in the progression to NASH, because it not only represses the expression of genes involved in fatty acids synthesis [15], but also antagonizes inflammation [57,58]. Indeed, studies conducted on various animal models have indicated that the induction of Nrf2 counteracts alcoholic and nonalcoholic liver disease by decreasing early inflammatory response [58,59].

Although a recent work on Nrf2^{-/-} macrophages have highlighted that Nrf2 is essential for Nlrp3 activation [60], it could be argued from many other literature data that a defective activity of the protective signaling pathway regulated by Nrf2 leads to enhanced Nlrp3 activation [19,20,61]. This inverse correlation between Nrf2 and Nlrp3 activation may thus play a role in the onset of chronic

inflammation contributing to the progression of NAFLD to NASH. Consistently, in HFRT fed mice we have found Nrf2 inhibition that could account, at least in part, for the observed Nlrp3 activation. Thus, an amplifying loop evoked by high-fats and high-sugars intake could be hypothesized to exist among SREBP, palmitate, Nrf2 and Nlrp3 that participate in the progression of liver diseases. On the basis of the above considerations, we can conclude that the peculiar alterations induced by fats and fructose on lipid metabolism differently affect antioxidant and proinflammatory pathways. In particular, the stronger SREBP1c activation induced by dietary fructose with respect to saturated fats, and the consequent palmitate production, are the leading factors responsible for the greater Nrf2 inhibition and Nlrp3 activation observed in HFRT mice livers, resulting in a more intense hepatic inflammatory response. These observations suggest that fructose may evoke a more rapid progression of NAFLD to NASH than fats, confirming that high fructose intake in western diet represents an important risk factor for health.

Disclosures

No conflict of interest, financial or otherwise, are declared by the authors.

References

[1] Bellentani S, Scaglioni F, Marino M, Bedogni G. Epidemiology of non-alcoholic fatty liver disease. Digestive Dis 2010; 28(1):155e61. doi: 10.1159/000282080.

[2] Cheung O, Sanyal AJ. Recent advances in nonalcoholic fatty liver disease. Curr Opin Gastroenterol 2010; 26(3):202e8. doi: 10.1097/MOG.0b013e328337b0c4.

[3] Jornayvaz FR, Shulman GI. Diacylglycerol activation of protein kinase cepsilon and hepatic insulin resistance. Cell Metabolism 2012; 15(5):574e84. doi: 10.1016/j.cmet.2012.03.005.

[4] Brownell KD, Farley T, Willett WC, Popkin BM, Chaloupka FJ, Thompson JW, Ludwig DS. The public health and economic benefits of taxing sugar-sweetened beverages. N Engl J Med 2009; 361(16):1599e605. doi: 10.1056/NEJMhpr0905723.

[5] Crescenzo R, Bianco F, Coppola P, Mazzoli A, Tussellino M, Carotenuto R, Liverini G, Iossa S. Fructose supplementation worsens the deleterious effects of short-term high-fat feeding on hepatic steatosis and lipid metabolism in adult rats. Exp Physiol 2014; 99(9):1203-13. doi: 10.1113/expphysiol.2014.079632.

[6] Fan JG, Cao HX. Role of diet and nutritional management in non-alcoholic fatty liver disease. J Gastroenterol Hepatol 2013; 28:81–7. doi: 10.1111/jgh.12244.

[7] Asrih M, Jornayvaz FR. Diets and nonalcoholic fatty liver disease: The good and the bad. Clin Nutr 2014; 33(2):186-90. doi: 10.1016/j.clnu.

[8] Lê KA, Ith M, Kreis R, Faeh D, Bortolotti M, Tran C, Boesch C, Tappy L. Fructose overconsumption causes dyslipidemia and ectopic lipid deposition in healthy subjects with and without a family history of type 2 diabetes. Am J Clin Nutr 2009; 89(6):1760-5. doi: 10.3945/ajcn.2008.27336.

[9] Desmarchelier C, Ludwig T, Scheundel R, Rink N, Bader BL, Klingenspor M, Daniel H. Diet-induced obesity in ad libitum-fed mice: food texture overrides the effect of macronutrient composition. Br J Nutr 2013; 109:1518–27. doi: 10.1017/S0007114512003340.

[10] Sellmann C, Priebs J, Landmann M, Degen C, Engstler AJ, Jin CJ, Gärttner S, Spruss A, Huber O, Bergheim I. Diets rich in fructose, fat or fructose and fat alter intestinal barrier function and lead to development of non-alcoholic fatty liver disease over time. J Nutr Biochem 2015; 26(11):1183-92. doi: 10.1016/j.jnutbio.2015.05.011.

[11] Ren LP, Chan SMH, Zeng XY, Laybutt DR, Iseli TJ, Sun RQ, Kraegen EW, Cooney GJ, Turner N & Ye JM. Differing endoplasmatic reticulum stress response to excess lipogenesis versus lipid oversupply in relation to hepatic steatosis and insulin resistance. PLoS ONE 2012; 7(2):e30816. doi: 10.1371/journal.pone.0030816.

[12] Peverill W, Powell LW, Skoien R. Evolving concepts in the pathogenesis of NASH: beyond steatosis and inflammation. Int J Mol Sci 2014;15(5):8591-638. doi: 10.3390/ijms15058591.

[13] Meakin PJ, Chowdhry S, Sharma RS, Ashford FB, Walsh SV, McCrimmon RJ, Dinkova-Kostova AT, Dillon JF, Hayes JD, Ashford ML. Susceptibility of Nrf2-null mice to steatohepatitis and cirrhosis upon consumption of a high-fat diet is associated with oxidative stress, perturbation of the unfolded protein response, and disturbance in the expression of metabolic enzymes but not with insulin resistance. Mol Cell Biol 2014; 34(17):3305-20. doi: 10.1128/MCB.00677-14.

[14] Valdecantos MP, Prieto-Hontoria PL, Pardo V, Módol T, Santamaría B, Weber M, Herrero L, Serra D, Muntané J, Cuadrado A, Moreno-Aliaga MJ, J, Martínez A, Valverde ÁM. Essential

role of Nrf2 in the protective effect of lipoic acid against lipoapoptosis in hepatocytes. Free Radic Biol Med 2015; 84(2015)263–278. doi: 10.1016/j.freeradbiomed.

[15] Kitteringham NR, Abdullah A, Walsh J, Randle L, Jenkins RE, Sison R, Goldring CE, Powell H, Sanderson C, Williams S, Higgins L, Yamamoto M, Hayes J, Park BK. Proteomic analysis of Nrf2 deficient transgenic mice reveals cellular defence and lipid metabolism as primary Nrf2-dependent pathways in the liver. J Proteomics 2010; 73(8):1612-31. doi: 10.1016/j.jprot.2010.03.018.

[16] Ludtmann MH, Angelova PR, Zhang Y, Abramov AY, Dinkova-Kostova AT. Nrf2 affects the efficiency of mitochondrial fatty acid oxidation. Biochem J 2014;457(3):415-24. doi: 10.1042/BJ20130863.

[17] Ramadori P, Drescher H, Erschfeld S, Schumacher F, Berger C, Fragoulis A, Schenkel J, Kensler TW, Wruck CJ, Trautwein C, Kroy DC, Streetz KL. Hepatocyte-specific Keap1 deletion reduces liver steatosis but not inflammation during non-alcoholic steatohepatitis development. Free Radic Biol Med 2016; 91:114-26. doi: 10.1016/j.freeradbiomed.2015.12.014.

[18] Liu X, Wang T, Liu X, Cai L, Qi J, Zhang P, Li Y. Biochanin A protects lipopolysaccharide/D-galactosamine-induced acute liver injury in mice by activating the Nrf2 pathway and inhibiting NLRP3 inflammasome activation. Int Immunopharmacol 2016;38:324-331. doi: 10.1016/j.intimp.2016.06.009.

[19] Cai SM, Yang RQ, Li Y, Ning ZW, Zhang LL, Zhou GS, Luo W, Li DH, Chen Y, Pan MX, Li X. Angiotensin-(1-7) Improves Liver Fibrosis by Regulating the NLRP3 Inflammasome via Redox Balance Modulation. Antioxid Redox Signal 2016; 10;24(14):795-812. doi: 10.1089/ars.2015.6498.

[20] Pan CW, Pan ZZ, Hu JJ, Chen WL, Zhou GY, Lin W, Jin LX, Xu CL. Mangiferin alleviates lipopolysaccharide and D-galactosamine-induced acute liver injury by activating the Nrf2pathway and inhibiting NLRP3 inflammasome activation. Eur J Pharmacol 2016, 5;770:85-91. doi: 10.1016/j.ejphar.

[21] Baiocchi C, Medana C, Dal Bello F, Giancotti V, Aigotti R and Gastaldi D. Analysis of regioisomers of polyunsaturated triacylglycerols in marine matrices by HPLC/HRMS. Food Chem 2015; 166: 551-560.

[22] Mastrocola R, Collino M, Rogazzo M, Medana C, Nigro D, Boccuzzi G, Aragno M. Advanced glycation end products promote hepatosteatosis by interfering with SCAP-SREBP pathway in fructose-drinking mice. Am J Physiol Gastrointest Liver Physiol 2013; 305(6):G398-407. doi: 10.1152/ajpgi.00450.

[23] Spinazzi M, Casarin A, Pertegato V, Salviati L, Angelini C. Assessment of mitochondrial respiratory chain enzymatic activities on tissues and cultured cells. Nat Protoc 2012; 7(6):1235-46. doi: 10.1038/nprot.2012.058.

[24] Owens CW, Belcher RV. A colorimetric micro-method for the determination of glutathione. Biochem J 1965; 94:705-11.

[25] Lau A, Tian W, Whitman SA, Zhang DD. The predicted molecular weight of Nrf2: it is what it is not. Antioxid Redox Signal 2013; 18(1):91-3. doi: 10.1089/ars.2012.4754.

[26] Ferramosca A, Zara V. Modulation of hepatic steatosis by dietary fatty acids. World J Gastroenterol 2014; 20:1746–55. doi: 10.3748/wjg.v20.i7.1746.

[27] Ouyang X, Cirillo P, Sautin Y, McCall S, Bruchette JL, Diehl AM, Johnson RJ, Abdelmalek MF. Fructose consumption as a risk factor for non-alcoholic fatty liver disease. J Hepatol 2008; 48:993–9. doi: 10.1016/j.jhep.2008.02.011.

[28] Stanhope KL, Schwarz JM, Keim NL, Griffen SC, Bremer AA, Graham JL, Hatcher B, Cox CL, Dyachenko A, Zhang W, McGahan JP, Seibert A, Krauss RM,Chiu S, Schaefer EJ, Ai M, Otokozawa S, Nakajima K, Nakano T, Beysen C, Hellerstein MK, Berglund L, Havel PJ. Consuming fructose-sweetened, not glucose-sweetened, beverages increases visceral adiposity and lipids and decreases insulin sensitivity in overweight/obese humans. J Clin Investig 2009; 119, 1322–1334. doi: 10.1172/JCI37385.

[29] Lim JS, Mietus-Snyder M, Valente A, Schwarz JM, Lustig RH. The role of fructose in the pathogenesis of NAFLD and the metabolic syndrome. Nat Rev Gastroenterol Hepatol 2010; 7(5):251-64. doi: 10.1038/nrgastro.2010.41

[30] Erion DM, Shulman GI. Diacylglycerol-mediated insulin resistance. Nat Med 2010; 16: 400–402. doi: 10.1038/nm0410-400.

[31] Mastrocola R, Nigro D, Chiazza F, Medana C, Dal Bello F, Boccuzzi G, Collino M, Aragno M. Fructose-derived advanced glycation end-products drive lipogenesis and skeletal muscle reprogramming via SREBP-1c dysregulation in mice. Free Radical Biol Med 2016; 91:224-35. doi: 10.1016/j.freeradbiomed.

[32] Schwarz JM, Noworolski SM, Wen MJ, Dyachenko A, Prior JL, Weinberg ME, Herraiz LA, Tai VW, Bergeron N, Bersot TP, Rao MN, Schambelan M,Mulligan K. Effect of a High-Fructose Weight-Maintaining Diet on Lipogenesis and Liver Fat. J Clin Endocrinol Metab 2015; 100(6):2434-42. doi: 10.1210/jc.2014-3678.

[33] Schultz A, Neil D, Aguila MB, Mandarim-de-Lacerda CA. Hepatic adverse effects of fructose consumption independent of overweight/obesity. Int J Mol Sci 2013; 5;14(11):21873-86. doi: 10.3390/ijms141121873.

[34] Schultz A, Barbosa-da-Silva S, Aguila MB, Mandarim-de-Lacerda CA. Differences and similarities in hepatic lipogenesis, gluconeogenesis and oxidative imbalance in mice fed diets rich in fructose or sucrose. Food Funct 2015; 6(5):1684-91. doi: 10.1039/c5fo00251f.

[35] Oakes ND, Kjellstedt A, Thal´en P, Ljung B, Turner N. Roles of fatty acid oversupply and impaired oxidation in lipid accumulation in tissues of obese rats. J Lipids 2013; 420754, 2013. doi: 10.1155/2013/420754.

[36] Ji H and Friedman MI. Reduced Capacity for Fatty Acid Oxidation in Rats with Inherited Susceptibility to Diet-Induced Obesity. Metabolism 2007; 56(8): 1124–1130. doi: 10.1016/j.metabol.2007.04.006

[37] Nagle CA, Klett EL and Coleman RA. Hepatic triacylglycerol accumulation and insulin resistance J Lipid Res 2009; 50(Suppl): S74–S79. doi: 10.1194/jlr.R800053-JLR200.

[38] Crescenzo R, Bianco F, Coppola P, Mazzoli A, Cigliano L, Liverini G, Iossa S. Increased skeletal muscle mitochondrial efficiency in rats with fructose-induced alteration in glucose tolerance. Br J Nutr 2013; 14;110(11):1996-2003. doi: 10.1017/S0007114513001566.

[39] Stanhope KL, Medici V, Bremer AA, Lee V, Lam HD, Nunez MV, Chen GX, Keim NL, Havel PJ. A dose-response study of consuming high-fructose corn syrup-sweetened beverages on lipid/lipoprotein risk factors for cardiovascular disease in young adults. Am J Clin Nutr 2015; 101(6):1144-54. doi: 10.3945/ajcn.114.100461.

[40] Kawano Y, Cohen DE. Mechanisms of hepatic triglyceride accumulation in non-alcoholic fatty liver disease. J Gastroenterol 2013; 48:434–441. doi: 10.1007/s00535-013-0758-5.

[41] Wu N, Sarna LK, Hwang SY, Zhu Q, Wang P, Siow YL, O K. Activation of 3-hydroxy-3-methylglutaryl coenzyme A (HMG-CoA) reductase during high fat diet feeding. Biochim Biophys Acta 2013; 1832(10):1560-8. doi: 10.1016/j.bbadis.

[42] Weigert C, Brodbeck K, Staiger H, Kausch C, Machicao F, Häring HU, Schleicher ED. Palmitate, but not unsaturated fatty acids, induces the expression of interleukin-6 in human myotubes through proteasome-dependent activation of nuclear factor-kappaB. J Biol Chem 2004; 4;279(23):23942-52.

[43] Schwartz EA, Zhang WY, Karnik SK, Borwege S, Anand VR, Laine PS, Su Y, Reaven PD. Nutrient modification of the innate immune response: a novel mechanism by which saturated fatty acids greatly amplify monocyte inflammation. Arterioscler Thromb Vasc Biol 2010; 30(4):802-8. doi: 10.1161/ATVBAHA.109.201681.

[44] Ma W, Wu JH, Wang Q, Lemaitre RN, Mukamal KJ, Djoussé L, King IB, Song X, Biggs L, Delaney JA, Kizer JR, Siscovick DS, Mozaffarian D. Prospective association of fatty acids in the de novo lipogenesis pathway with risk of type 2 diabetes: the Cardiovascular Health Study. Am J Clin Nutr 2015; 101(1):153-63. doi: 10.3945/ajcn.114.092601.

[45] Wree A, McGeough MD, Peña CA, Schlattjan M, Li H, Inzaugarat ME, Messer K, Canbay A, Hoffman HM, Feldstein AE. NLRP3 inflammasome activation is required for fibrosis development in NAFLD. J Mol Med (Berl) 2014; 92(10):1069-82. doi: 10.1007/s00109-014-1170-1.

[46] Csak T, Ganz M, Pespisa J, Kodys K, Dolganiuc A, Szabo G. Fatty acid and endotoxin activate inflammasomes in mouse hepatocytes that release danger signals to stimulate immune cells. Hepatology 2010; 54:133–144. doi: 10.1002/hep.24341.

[47] Csak T, Pillai A, Ganz M, Lippai D, Petrasek J, Park JK, Kodys K, Dolganiuc A, Kurt-Jones EA, Szabo G. Both bone marrow-derived and non-bone marrow-derived cells contribute to AIM2 and NLRP3 inflammasome activation in a MyD88-dependent manner in dietary steatohepatitis. Liver Int. 2014 Oct;34(9):1402-13. doi: 10.1111/liv.12537. Epub 2014 Apr 17.

[48] Chiazza F, Couturier-Maillard A, Benetti E, Mastrocola R, Nigro D, Cutrin JC, Serpe L, Aragno M, Fantozzi R, Ryffel B, Thiemermann C, Collino M. Targeting the NLRP3 inflammasome to reduce diet-induced metabolic abnormalities in mice. Mol Med. 2015 Nov 23. doi: 10.2119/molmed.2015.00104.

[49] Collino M, Benetti E, Rogazzo M, Mastrocola R, Yaqoob MM, Aragno M, Thiemermann C, Fantozzi R. Reversal of the deleterious effects of chronic dietary HFCS-55 intake by PPAR-δ agonism correlates with impaired NLRP3 inflammasome activation. Biochem Pharmacol. 2013 Jan 15;85(2):257-64. doi: 10.1016/j.bcp.2012.10.014.

[50] Im SS, Yousef L, Blaschitz C, Liu JZ, Edwards RA. Linking lipid metabolism to the innate immune response in macrophages through Sterol Regulatory Element Binding Protein-1a. Cell Metab 2011; 13: 540–549. doi: 10.1016/j.cmet.2011.04.001.

[51] Xiao H, Lu M, Lin TY, Chen Z, Chen G, Wang WC, Marin T, Shentu TP, Wen L, Gongol B, Sun W, Liang X, Chen J, Huang HD, Pedra JHF, Johnson DA, Shyy JYJ. Sterol regulatory element binding protein 2 activation of NLRP3 inflammasome in endothelium mediates hemodynamicinduced atherosclerosis susceptibility. Circulation 2013; 128:632–642. doi: 10.1161/CIRCULATIONAHA.113.002714.

[52] Hayes JD and Dinkova-Kostova AT. The Nrf2 regulatory network provides an interface between redox and intermediary metabolism. Trends Biochem Sciences 2014; vol. 39, no. 4, pp. 199–218. doi: 10.1016/j.tibs.2014.02.002.

[53] Cui Y, Wang Q, Yi X, Zhang X. Effects of Fatty Acids on CYP2A5 and Nrf2 Expression in Mouse Primary Hepatocytes. Biochem Genet 2016; 54(1):29-40. doi: 10.1007/s10528-015-9697-6.

[54] Wang X, Liu JZ, Hu JX, Wu H, Li YL, Chen HL, Bai H, Hai CX. ROS-activated p38 MAPK/ERK-Akt cascade plays a central role in palmitic acid-stimulated hepatocyte proliferation. Free Radic Biol Med 2011; 51(2):539-51. doi:10.1016/j.freeradbiomed.2011.04.019.

[55] Fratantonio D, Speciale A, Ferrari D, Cristani M, Saija A, Cimino F. Palmitate-induced endothelial dysfunction is attenuated by cyanidin-3-O-glucoside through modulation of Nrf2/Bach1 and NF-κB pathways. Toxicol Lett 2015; 15;239(3):152-60. doi: 10.1016/j.toxlet.2015.09.020.

[56] Chanas SA, Jiang Q, McMahon M, McWalter GK, McLellan LI, Elcombe CR, Henderson CJ, Wolf CR, Moffat GJ, Itoh K, Yamamoto M, Hayes JD. Loss of the Nrf2 transcription factor causes a marked reduction in constitutive and inducible expression of the glutathione S-transferase Gsta1, Gsta2, Gstm1, Gstm2, Gstm3 and Gstm4 genes in the livers of male and female mice. Biochem J 2002; 365(Pt 2):405-16.

[57] Reddy NM, Potteti HR, Mariani TJ, Biswal S, Reddy SP. Conditional deletion of Nrf2 in airway epithelium exacerbates acute lung injury and impairs the resolution of inflammation. Am J Respir Cell Mol Biol 2011; 45:1161–1168. doi: 10.1165/rcmb.2011-0144OC.

[58] Shin SM, Yang JH, Ki SH. Role of the Nrf2-ARE pathway in liver diseases. Oxid Med Cell Longev 2013; 2013:763257. doi: 10.1155/2013/763257.

[59] Lee LY, Köhler UA, Zhang L, Roenneburg D, Werner S, Johnson JA, Foley DP. Activation of the Nrf2-ARE pathway in hepatocytes protects against steatosis in nutritionally induced non-alcoholic steatohepatitis in mice. Toxicol Sci 2014; 142(2):361-74. doi: 10.1093/toxsci/kfu184.

[60] Zhao C, Gillette DD, Li X, Zhang Z, Wen H. Nuclear factor E2-related factor-2 (Nrf2) is required for NLRP3 and AIM2 inflammasome activation. J Biol Chem 2014; 13;289(24):17020-9. doi: 10.1074/jbc.M114.563114.

[61] Gao YZ, Zhao LF, Ma J, Xue WH, Zhao H. Protective mechanisms of wogonoside against Lipopolysaccharide/d-galactosamine-induced acute liver injury in mice. Eur J Pharmacol 2016; 5;780:8-15. doi: 10.1016/j.ejphar.2016.02.040.

Table 1. Characteristics of diet intake of mice fed a standard (SD), a high-fat (HFAT), and a high-fructose (HFRT) diet for 12 weeks. Data are means ± s.e.m. Statistical significance: [a]$P<0.05$, [b]$P<0.001$ vs SD; [c]$P<0.05$, [d]$P<0.001$ vs HFAT.

	SD (n=8)	HFAT (n=10)	HFRT (n=10)
Diet energy supply (Kcal/g)	3.85	4.70	3.85
Food intake (g/day/mouse)	2.48 ± 0.09	2.58 ± 0.15	2.65 ± 0.07
Total calories intake (Kcal/day/mouse)	9.6 ± 0.4	12.1 ± 0.7[a]	10.2 ± 0.3[c]
Fat calories intake (Kcal/day/mouse)	0.43 ± 0.05	5.46 ± 0.32[b]	0.46 ± 0.01[d]
Sugar calories intake (Kcal/day/mouse)	0.00 ± 0.00	2.06 ± 0.12[a]	6.13 ± 0.26[b,d]

Table 2. Physiological parameters of mice after 12 weeks of standard, high-fat, and high-fructose diet. Data are means ± s.e.m. Statistical significance: [a]$P<0.05$, [b]$P<0.001$ vs SD; [c]$P<0.05$, [d]$P<0.001$ vs HFAT.

	SD (n=8)	HFAT (n=10)	HFRT (n=10)
Body weight increase (g)	8.5 ± 1.6	17.2 ± 4.6[b]	8.3 ± 1.5[d]
Liver weight (% of body w.)	3.5 ± 0.2	2.7 ± 0.4[b]	3.6 ± 0.1[d]
Epididimal weight (% of body w.)	1.2 ± 0.4	6.1 ± 0.9[b]	1.5 ± 0.4[d]
Systolic pressure (mm Hg)	112 ± 7	106 ± 11	113 ± 3
Fasting glyceamia (mg/dL)	69 ± 19	120 ± 21[a]	91 ± 11[a,c]
Insulinemia (mg/dL)	85.8 ± 5.3	106.0 ± 12.6[a]	86.6 ± 7.1[c]
Plasma TG (mg/dL)	30.7 ± 6.6	86.3 ± 27.8[b]	45.5 ± 5.0[a]
Plasma cholesterol (mg/dL)	77.2 ± 5.7	267.1 ± 94.6[b]	115.3 ± 12.5[a,c]

Table 3. TAGs composition evaluated by LC-MS analysis on liver homogenates. Data are means ± s.e.m. Statistical significance: [a]$P<0.05$, [b]$P<0.001$ vs SD; [c]$P<0.05$, [d]$P<0.001$ vs HFAT. Fatty acids identification: L: linoleic; Ln: linolenic; M: myristic; O: oleic; P: palmitic; Po: palmitoleic; S: stearic.

TAGs (% of total)	SD (n=8)	HFAT (n=10)	HFRT (n=10)
L-Ln-O	4.13 ± 0.41	4.86 ± 0.23	2.96 ± 0.28[a,d]
L-L-O	14.07 ± 2.43	12.91 ± 0.51	10.13 ± 1.06
Po-O-M	0.48 ± 0.06	0.45 ± 0.01	0.36 ± 0.06
Po-S-Ln	3.11 ± 0.69	4.28 ± 0.07	3.12 ± 0.56
O-O-L	22.19 ± 2.22	21.51 ± 0.89	19.87 ± 1.50
P-L-O	7.11 ± 0.60	7.09 ± 0.40	19.92 ± 2.32[b,d]
M-P-O	0.95 ± 0.17	0.98 ± 0.04	0.68 ± 0.11
O-O-O	26.84 ± 3.33	27.61 ± 1.02	20.03 ± 2.92
P-P-O	3.18 ± 0.21	2.48 ± 0.07[a]	2.26 ± 0.22[b]
O-O-P	8.27 ± 0.87	7.41 ± 0.20	12.14 ± 1.16[a]
P-O-S	2.66 ± 0.08	2.85 ± 0.11	3.16 ± 0.15[a]
O-O-S	2.55 ± 0.23	3.18 ± 0.07	2.01 ± 0.2[d]
S-S-O	4.49 ± 0.51	4.39 ± 0.17	3.36 ± 0.60

Figure legends

Figure 1. Oral glucose tolerance test (OGTT). Oral glucose tolerance test performed on mice fed a standard (SD), a high-fat (HFAT) or a high-fructose (HFRT) diet. Data are mean ± s.e.m of 8-10 mice for group. Statistical significance: [a]$P<0.05$ vs SD; [b]$P<0.001$ vs SD; [c]$P<0.05$ vs HFAT; [d]$P<0.001$ vs HFAT.

Figure 2. Lipids deposition in liver. (a) Representative 20X magnification photomicrographs of Oil Red O staining on liver sections from SD, HFAT and HFRT fed mice. (b) Triglyceride (TG) and cholesterol content in mice liver. Data are mean ± s.e.m of 8-10 mice for group. Statistical significance: [a]$P<0.05$ vs SD; [b]$P<0.001$ vs SD; [d]$P<0.001$ vs HFAT.

Figure 3. Markers of TG export and mitochondrial biogenesis and β-oxidation in liver. Representative western blotting analysis performed in liver cytosolic extracts for ApoB (a), CPT1-l (b), PGC-1α (c), SDHA and COX1 (d). Histograms report densitometric analyses normalized for the relative GAPDH content. Data are mean ± s.e.m of 8-10 mice for group. Statistical significance: [a]$P<0.05$ vs SD; [b]$P<0.001$ vs SD; [c]$P<0.05$ vs HFAT; [d]$P<0.001$ vs HFAT.

Figure 4. Activities of mitochondrial respiration complexes in liver. Mitochondrial respiration complexes enzymatic activities were assessed in liver homogenates from SD, HFAT and HFRT mice. (a) complex I, ubiquinone oxidoreductase; (b) complex II, succinate dehydrogenase; (c) complex III, decyl ubiquinol cytochrome c oxidoreductase; (d) complex IV, cytochrome c oxidase. Data are mean ± s.e.m of 8-10 mice for group. Statistical significance: [b]$P<0.001$ vs SD; [c]$P<0.05$ vs HFAT; [d]$P<0.001$ vs HFAT.

Figure 5. Analysis of SCAP/SREBP pathway. Representative western blotting analysis performed in liver cytosolic and nuclear extracts for (a) SCAP and (b) SREBP1c. (c) mRNA expression levels
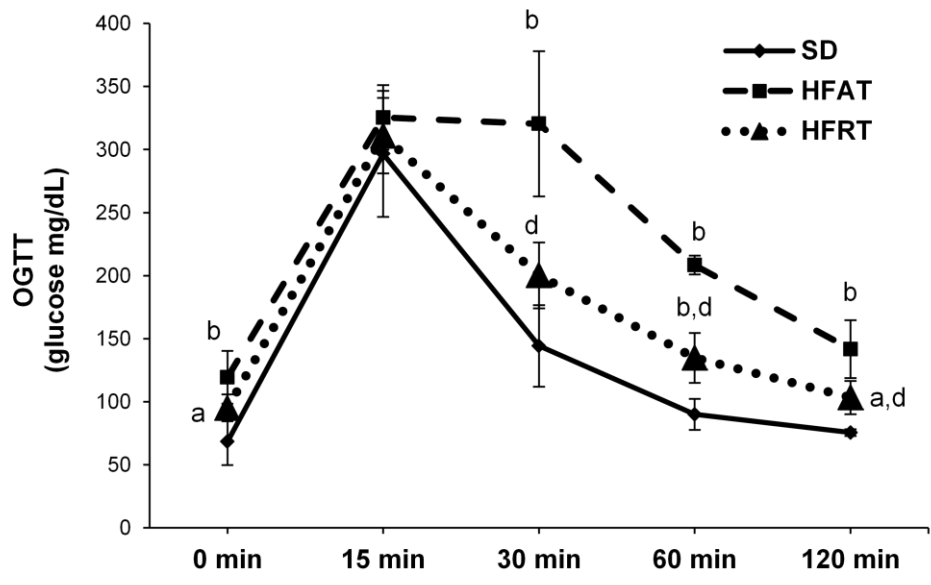
27

of ACC and FAS, and western blotting for protein levels of ACC, pACC and FAS. (d) Representative western blotting for cytosolic and nuclear levels of SREBP2. (e) mRNA expression levels and western blotting for protein levels of HMG-CoA-R. For RT-PCR analysis histograms report $2^{-\Delta\Delta Ct}$ values normalized for the relative RNR18S housekeeping gene. For western blotting analysis histograms report densitometric analyses normalized for the relative GAPDH and histone H3 content, in cytosolic and nuclear extracts, respectively. Data are mean $\pm$ s.e.m of 8-10 mice for group. Statistical significance: [a]$P<0.05$ vs SD; [b]$P<0.001$ vs SD; [d]$P<0.001$ vs HFAT.

Figure 6. Analysis of Keap1/Nrf2 pathway. Representative western blotting analysis performed in liver extracts for (a) cytosolic Keap1 and Nrf2 protein expression, and nuclear Nrf2 content. Histograms report densitometric analysis of Keap1 and of the 110-kDa band for Nrf2, normalized for the relative GAPDH and histone H3 content, in cytosolic and nuclear extracts, respectively. (b) Representative 40x micrographs of immunofluorescence analysis for subcellular localization of Nrf2 (red fluorescence) in liver cryostatic sections. Nuclei are stained in Hoechst blue dye. Enlarged details are shown in square boxes. (c) RT-PCR analysis on Nrf2 target genes performed in liver mRNA extracts. Histograms report $2^{-\Delta\Delta Ct}$ values normalized for the relative RNR18S housekeeping gene. (d) GSSG/GSH ratio assessed in cytosolic liver extracts. Data are mean $\pm$ s.e.m of 8-10 mice for group. Statistical significance: [b]$P<0.001$ vs SD; [c]$P<0.05$ vs HFAT; [d]$P<0.001$ vs HFAT.

Figure 7. Analysis of Nlrp3 inflammasome signalling. Representative western blotting analysis performed in liver for (a) Nlrp3 expression, (b) Pro-Caspase1 expression and cleavage, (c) active IL-1β, and (d) NFkB cytosolic and nuclear levels. Histograms report densitometric analysis normalized for the relative GAPDH and histone H3 content, in cytosolic and nuclear extracts, respectively. Data are mean $\pm$ s.e.m of 8-10 mice for group. Statistical significance: [b]$P<0.001$ vs SD; [c]$P<0.05$ vs HFAT; [d]$P<0.001$ vs HFAT.
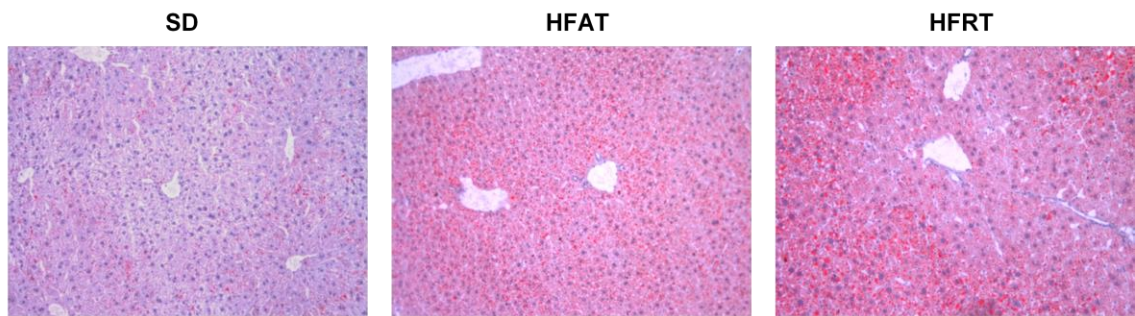
Figure 8. Markers of hepatic inflammation. (a) Representative western blotting analysis performed in liver cytosolic extracts for ICAM-1 protein levels. Histogram reports densitometric analysis normalized for the relative GAPDH. Data are mean ± s.e.m of 8-10 mice for group. Statistical significance: [a]$P<0.05$ vs SD; [c]$P<0.05$ vs HFAT. (b) Representative 10/20X magnification photomicrographs of immunohistochemistry for MPO on 10 μm cryostatic liver sections.
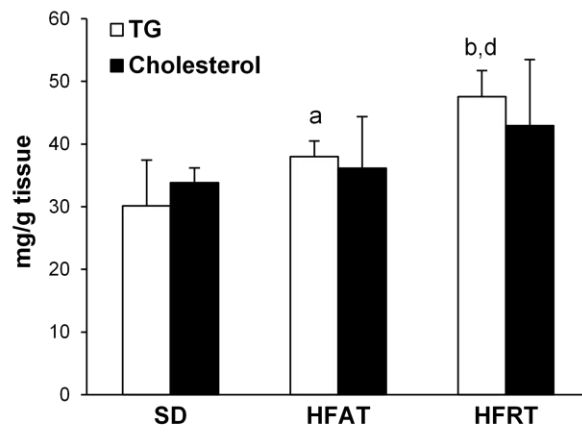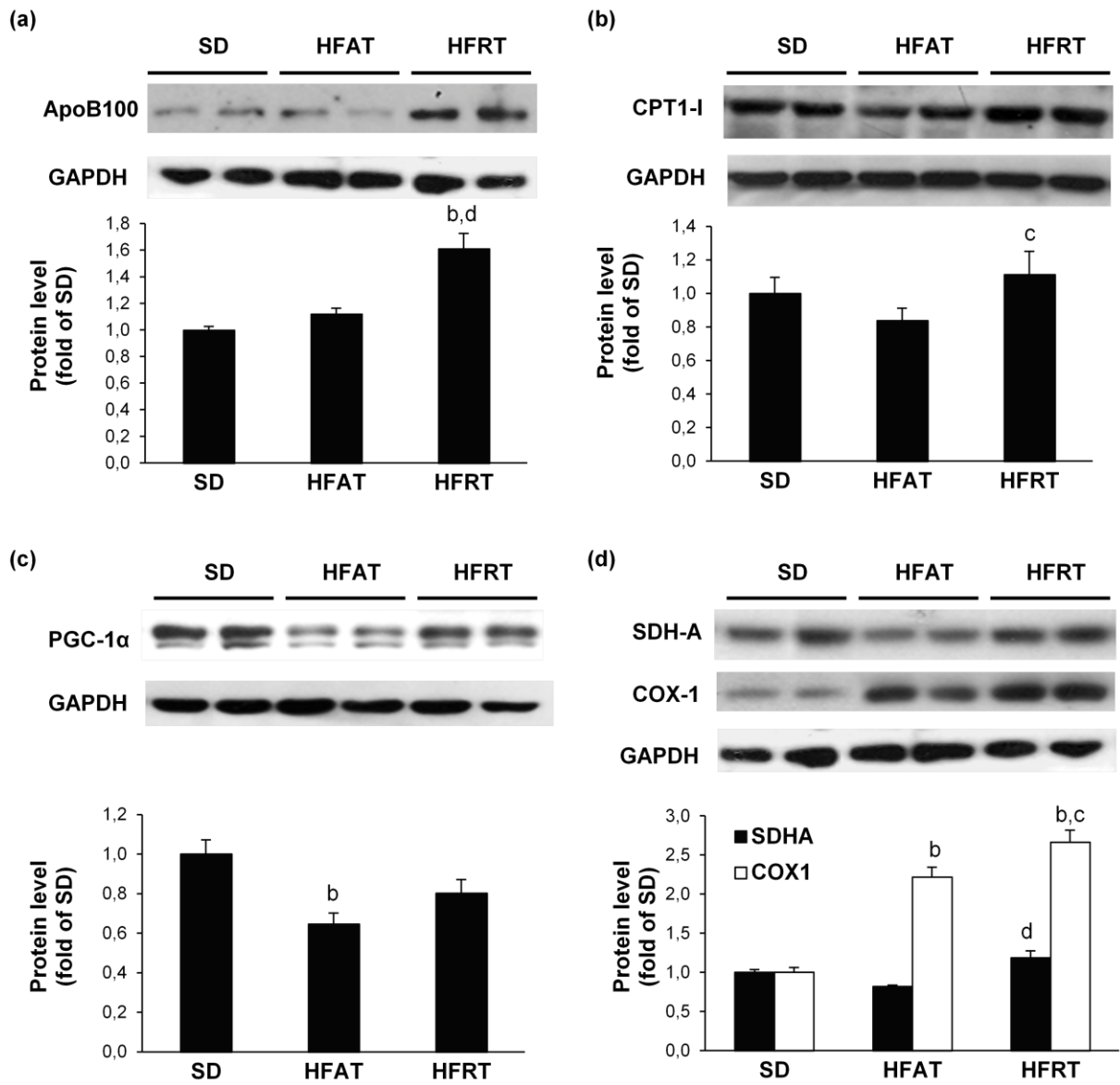
Fig. 1

Fig. 2

(a)

SD   HFAT   HFRT

(b)

Fig. 3

Fig. 4

(a) Complex I (△ABS/min/mg prot) — SD, HFAT (a), HFRT (b,d)

(b) Complex II (△ABS/min/mg prot) — CTRL, HFAT, HFRT (b,d)

(c) Complex III (△ABS/min/mg prot) — SD, HFAT, HFRT (b,c)

(d) Complex IV (△ABS/min/mg prot) — SD, HFAT, HFRT (b,d)

Fig. 5

(a)

(b)

(c)

(d)

(e)

Fig. 6

(a)

(b)

(c)

(d)

Fig. 7

(a)

SD   HFAT   HFRT

Nlrp3

GAPDH

(b)

SD   HFAT   HFRT

Pro-Caspase1

Caspase 1

GAPDH

(c)

SD   HFAT   HFRT

IL-1β

GAPDH

(d)

SD   HFAT   HFRT

Cytosolic NFkB p65

GAPDH

Nuclear NFkB p65

Histone H3

36

Fig. 8

(a)

(b)